Enhanced Molecular Fluorescence near Thick Ag Island Film of Large Pseudotabular Nanoparticles

Mitsuo Kawasaki* and Shuki Mine

Department of Molecular Engineering, Graduate School of Engineering, Kyoto University, Katsura, Kyoto 615-8510, Japan

Received: June 13, 2005; In Final Form: July 20, 2005

A highly reflective thick Ag island film (TAIF) sputter-grown on mica, consisting of unique large pseudotabular nanoislands, 60−200 nm across and 30−60 nm thick, produced an unusually strong surface enhanced fluorescence (SEF) for rhodamine dyes situated very close to (only ∼10 Å away from) the metal surface. A significantly greater part of the enhanced fluorescence was emitted into the back half space through TAIF and the mica substrate. The detailed fluorescence angular distribution was very similar to that of the light scattering by TAIF, suggesting that the enhanced emission originated from some large induced dipoles in TAIF. For reference, we also present a quantitative analysis of the fluorescent behavior of the same dye but directly coated on a reference glass surface. TAIF showed no distinct dipolar surface plasmon-like bands for excitation at normal incidence, and the light absorption by dye-coated TAIF could be described by simple superposition of the contribution of TAIF and that of the surface-bound dyes. However, the net dye absorptance was increased by 4−5 times due to the strong interactions of the dye transition dipoles with the TAIF-scattered fields. The estimated SEF quantum yield in the low dye coverage limit suggests a markedly high radiative yield of the induced dipole in TAIF around ∼0.5.

Introduction

The enhanced molecular fluorescence near the surfaces of metallic colloids and islands, a phenomenon closely related to the surface enhanced Raman scattering (SERS), represents one of the most impressive effects of roughened metallic surfaces on the optical properties of nearby molecules. The basic physical principles of the surface enhanced fluorescence (SEF) seem to have been well established in the early 1980s,[1−7] but there have been some continued efforts to gain further optimization and control over the metal−molecule interactions for SEF,[8−18] which are important for such potential applications of SEF as to biosensing and to biomedical testing.

Unlike SERS, which is an instantaneous inelastic scattering process, SEF involves a real excited molecular state. Thus, when the distance, d, between the fluorophores and the metal surface becomes too small, the radiative yield generally tends to be strongly reduced by rapid radiationless energy transfer to the metal (obeying d^{-3} law[19]) during the finite lifetime of the excited molecular state. As a result, it has been shown that SEF only works for low quantum yield fluorophores preferably placed at certain significant distances, 30−100 Å or more,[7−10,12−17] from the metal surface. However, the metal−molecule interactions in the photoexcitation and the follow-up processes including this short-ranged dye-to-metal energy transfer are expected to depend strongly on the natures of the metallic colloids or islands, and there seems still to be some room for further system modification.

In this article, we quantitatively address an unusually strong SEF for rhodamine dyes situated very close to (only 5−14 Å away from) the surface of highly reflective thick Ag island films (hereafter referred to as TAIF) sputter-grown on a mica substrate. This novel film consists of a dense monolayer of large pseudotabular Ag nanoislands 60−200 nm across and 30−60 nm thick (see Figure 1). Recently, Lakowicz and co-workers have suggested that larger Ag islands can indeed have higher SEF capabilities with the optimum size near 40 nm.[17,18] However, not only the large island size that may be even beyond this regime but also the unique morphology and, in particular, the markedly short-ranged SEF distinguish TAIF from the systems hitherto known.

As suggested by Nitzan and co-workers in their early theoretical studies of the surface-induced enhancement effects including SERS,[3,6] an important part of the enhanced fluorescent emission near the metal colloids or islands may be viewed as originating from the radiative part of the local electronic oscillation (or the local plasmon resonance) in the metal particle as excited by the molecular-emission dipole. The radiating plasmon model recently proposed by Lakowicz[18] basically follows the same concept. The efficiency of SEF then crucially depends on the radiative yield of this induced free electron motion, but it normally tends not to be so large because the metal also provides strongly nonradiative decay channels associated with the Joule heating. One finds an analogous situation in the radiative decay process of a plasmon surface polariton (PSP) that can be excited in continuous metal films. The PSP modes are known to produce a strongly directional and polarized light emission by coupling to the outgoing photons in some preferential directions satisfying the momentum conservation rule.[20−24] Such PSP modes can also be excited by the long-range coupling with molecular-emission dipoles.[20,21,23] However, the early experimental study of Moreland and co-workers[22] suggested that the radiative yield of PSP was typically ∼0.1 or less unless the Ag films had been grown on holographic gratings (where the radiative yield could reach as high as ∼0.8). The resonant free electron motion in Ag islands is different from

* To whom correspondence should be addressed. E-mail: Kawasaki@ap6.kuic.kyoto-u.ac.jp. Tel(fax): (+81)-75-383-2574.

10.1021/jp053167t CCC: $30.25
Published on Web 08/18/2005

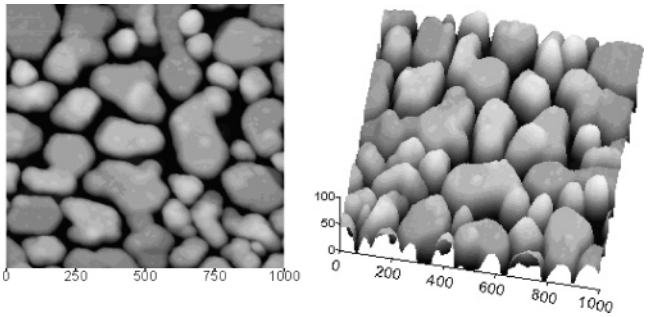

Figure 1. Typical AFM images (1×1 μm^2) of TAIF in top view (left) and in three-dimensional view (right) showing the large dimensions and unique morphology of the Ag nanoislands. Scales are in nm.

PSP in that the former is confined in the small dimensions of the metal particle, but whether it decays radiatively or nonradiatively will likewise depend strongly on the natures of the islands and their surroundings. The highly efficient and short-ranged SEF in dye-coated TAIF reported in this paper offers the unique opportunity to gain a quantitative estimate of the radiative yield for such induced dipoles and thereby strengthens that careful control of the morphology and dimensions of Ag islands can indeed allow some highly radiative local electromagnetic modes to be effectively excited by the nearby dye-emission dipoles.

In this paper, we also present a detailed comparative analysis of the fluorescence behavior of the same dyes but coated on a reference glass surface. This kind of nonmetallic surface has been commonly chosen as the reference surface without SEF, but the emission from molecular dipoles located at such a solid/air interface (an interface of refractive index discontinuity) is actually much more complex than the fluorescent emission in solution. Nevertheless, the corresponding fluorescence angular distribution can be exactly formulated by the available theory. The control experiment with the glass surface allows us to confirm that our experimental methods are capable to quantitatively reproduce such theoretical predictions, which in turn provides the important information of the absolute fluorescence quantum yield in the reference system. An additional attempt to obtain the reference fluorescence signals in combination with atomically smooth Ag(111) films yielded no more useful information, merely letting us reconfirm the strong quenching by the smooth metal surface that almost completely eliminated the measurable fluorescence signal in the conditions of interest.

The dye specifically focused on in this paper is rhodamine B (RhB), which is known to exhibit a high fluorescence quantum yield in sufficiently dilute solution[25] but be subject to strong self-quenching when deposited on solid surfaces depending on the dye coverage.[26] Thus simply by the coverage adjustment, we can examine a wide range of different quantum yield states subject to the short-ranged SEF by TAIF. We have also examined rhodamine 6G (R-6G), but the results were essentially identical.

Experimental Section

Materials and Sample Preparation. TAIFs were grown on freshly cleaved natural mica (purchased from The Nilaco Corporation) by the direct-current Ar^+-ion sputtering method in the same apparatus as used elsewhere for preparation of atomically flat Ag(111) and Au(111) films,[27,28] at a considerably high substrate temperature of 200−300 °C and a low deposition rate of 1−2 nm/min. Figure 1 shows a typical atomic force microscopy (AFM) image of TAIF (taken at Toray Research Center, Inc. with a Nanoscope IIIa microscope) grown by ∼30 min deposition in the above conditions. The film consists of large discrete nanoislands with a unique pseudotabular shape, 60−200 nm in lateral dimensions and 30−60 nm in height.

As the reference substrates without SEF we examined a cleaved mica surface, a borosilicate glass slide, and a quartz glass slide. Of these, the latter two substrates gave almost identical results, whereas the mica surface caused apparently stronger additional quenching to prevent a detailed analysis of the fluorescence angular dependence. We therefore chose the simple glass surface (ultrasonic cleaned in ethanol) as the common reference in what follows.

As for the molecular spacer layers to separate the dye molecules from the metallic surface for controlled distances, we employed the self-assembled monolayers or multilayers of mercaptocarboxylic acid compounds (obtained from Aldrich or from Wako Pure Chemical Industries, Ltd.). A simple immersion (for typically 10 min at room temperature) of the Ag film in 0.1 mM ethanolic solution of mercaptopropionic acid, thiosalicylic acid, or 11-mercaptoundecanoic acid allowed us to make approximately 4−14 Å thick self-assembled monolayers (assuming the vertically standing-up molecular orientation) terminated by −COOH groups. Thicker spacer layers, which are also terminated by −COOH groups, were prepared according to the multilayer self-assembly technique developed by Evans and coworkers,[29] via sequential adsorption of 11-mercaptoundecanoic acid (from 0.1-mM ethanolic solution) and Cu^{2+} ions (from 1 mM ethanolic solution of $Cu(ClO_4)_2$), each for 10 min at room temperature with an intermediate thorough washing with ethanol. The expected change in the average thickness with the number of layers was examined by X-ray photoelectron spectroscopy (XPS) analysis with an ESCA-750 spectrometer (Shimadzu Corp.). This is based on the exponential intensity attenuation of the Ag_{3d} XPS signal from the Ag film underneath with the spacer thickness. The result suggested that the average thickness of the multilayers increased in the same fashion as found on gold for approximately ∼14 Å per each monolayer.[29]

RhB and R-6G were obtained from Lambda Physik, Inc. Deposition of these dyes onto the sample surface was carried out by using the spin coating (at 3000 rpm) method, where 0.1 mL of ethanolic dye solution in the concentration range, 0.001−0.3 mM, was spun on the sample surface typically $\sim 12 \times 12$ mm^2 in area. This method resulted in highly uniform and reproducible dye coverage on all kinds of solid surfaces examined in this work. In addition, the total amount of the dye deposited per unit area, determined by an ethanolic extraction followed by the standard spectrophotometric quantification, was found to have a good linear relationship with the dye concentration in the spun solution.

Spectroscopic Measurements. The specular transmission and reflection spectra (at normal incidence) of all kinds of samples were acquired by using a home-assembled microscopic spectrometer system comprising a Nikon microscope, a multichannel analyzer (Hamamatsu Photonics, PMA-11), and two independent halogen lamps for the transmission and reflection measurements. The area of the sample probed in this microscopic measurement was less than 1 mm in diameter. The absolute specular reflectance (R) was measured by referring to that (0.08) of a borosilicate cover glass determined from its transmittance (T) according to $R = 1 - T$, which is valid for samples with negligible absorption and scattering. This reference reflectance also agreed with that calculated from the glass refractive index (1.51) taking multiple reflections into account.

The experimental setup used for the quantitative fluorescence measurement and also to obtain the scattering spectra is shown

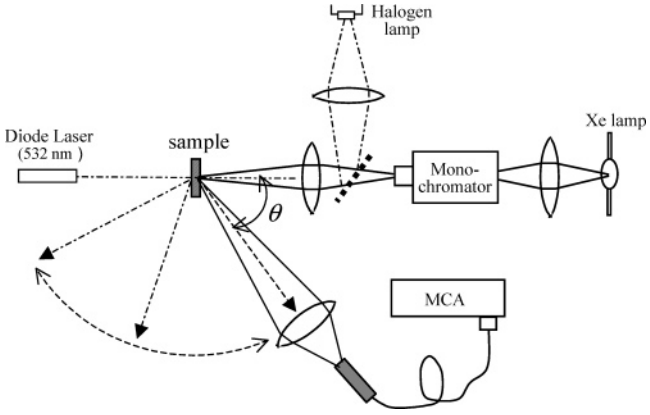

Figure 2. Experimental setup for angle-resolved fluorescence measurement and for the measurement of scattering spectra. MCA stands for a multichannel analyzer.

in Figure 2 (top view). The main light source for the fluorescence excitation was a 150-W Xe lamp, combined with a monochromator so that the output light from the exit slit (with purity better than 10 nm) was focused onto the sample surface with a rectangular spot size of $\sim 1 \times 3$ mm^2, corresponding to the average excitation light power of the order of 10 mW/cm^2. We additionally used a green (532 nm) diode laser (depolarized, $\sim$60 mW/cm^2 with a spot size of $\sim$1 mm in diameter) in the configuration as shown in Figure 2. In either case, we always made the front side of the sample (the side with the metal film and/or the deposited dye) face the excitation light at normal incidence. Another light source shown in Figure 2 is a 100-W halogen lamp used to obtain the scattering spectra. The corresponding white light was focused onto the sample surface with the common focusing lens to a spot size of $\sim$2 mm in diameter again at normal incidence.

The fluorescent light (or scattered light) was collected by the use of a camera lens (Pentax, $f = 50$ mm) with a 3-cm aperture, located 11 cm away from the sample, and then focused onto the small aperture ($\sim$2 mm) of the light receiver head of a multichannel analyzer (PMA-11). This whole subunit for light collection was made rotatable over some wide range of polar angle (θ), 30$-$160°, at which the light collection lens viewed the sample. In this geometry, the small irradiated spot of the sample can be treated as a point source, and the above light collection lens subtended a small solid angle of $\sim$0.06 steradian ($\sim$0.5% of the total solid angle of 4π). This allowed a fairly accurate measurement of the fluorescent angular dependence and that of the scattering, though at the considerable expense of light detection efficiency.

Absolute Efficiency Measurement and System Calibration. The absolute efficiencies of fluorescence and scattering were estimated based on the above-noted angular dependence relative to that of the scattering from a pellet made of fine ($\sim$50 nm) MgO powders (obtained from Wako Pure Chemical Industries, Ltd.). The MgO scatterer can be assumed to be an ideal diffuse reflector with the total integrated reflectance close to unity (0.97$-$0.98) in the visible region[30] and with the angular dependence of the diffuse-reflected light obeying the following Lambert's cosine law[31]

$$I(\theta) = I_0 \cos\theta \quad (0 \le \theta \le \pi/2) \tag{1}$$

We confirmed that this law was satisfied well in our experimental setup. The fluorescence and scattering from the sample also diffuse out into the backspace of the sample, but once their respective angular dependences were known, their absolute efficiencies can be calculated in a straightforward manner. The validity of this procedure was checked by measuring the fluorescence quantum yield of a sufficiently dilute (of the order of 10^{-6} M) ethanolic solution of R-6G put in a thin quartz optical cell (1-mm light path length). R-6G in ethanol is one of the best quantum yield standards with the recommended yield of 0.95.[32] The net light absorptance of the sample solution at the excitation wavelength at normal incidence was measured separately. For this solution sample, the fluorescence was emitted symmetrically into the front and backspaces of the thin quartz cell, with the following expected angular dependence convolving the refraction effect[31]

$$I(\theta) = I_0|\cos\theta|/n(n^2 - \sin^2\theta)^{1/2} \tag{2}$$

Here, n represents the refractive index of the solvent (1.36 for ethanol). The absolute fluorescence quantum yield of the R-6G solution estimated based on this angular dependence was 0.99. The discrepancy from the recommended standard yield was less than 5%. This verifies the capability of our angle-resolved fluorometer to yield sufficiently quantitative experimental information.

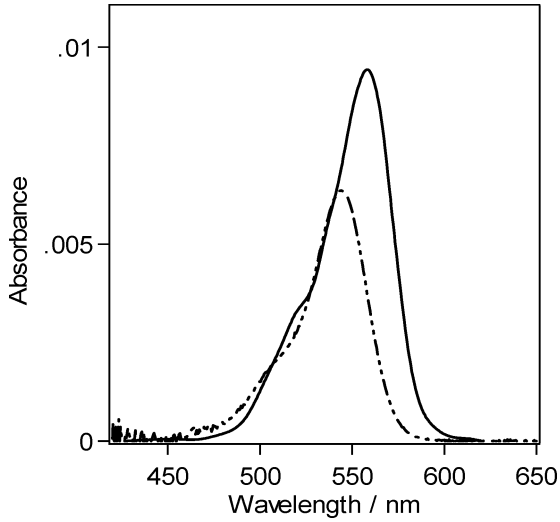

Figure 3. Comparison between the absorption spectrum of RhB on glass (solid curve) and that in ethanolic solution (dashed line) for the same number of dye molecules per unit area, 3.9×10^{13} molecules/cm^2.

Results and Discussion

Dye Fluorescence on Reference Substrate. When the fluorophores are surface bound at the interface constituting a refractive index discontinuity, one encounters an extra complexity. In such a case, it is known that a considerably greater part of the fluorescence is emitted into the medium of a higher refractive index,[33,34] with a unique angular dependence peaked at the critical angle (the angle of total internal reflection).[34] The angular dependence also depends strongly on the orientation of the surface-bound emission dipole. It is prudent to see first of all how closely the fluorescence from dyes deposited directly on the reference glass surface follows these general predictions in our experimental conditions. To do so, we first need to know the extent of preferential molecular orientation of the surface-bound RhBs.

In Figure 3, a noticeably red-shifted and somewhat broadened absorption spectrum of RhB spun on the glass surface (at the coverage of 3.9×10^{13} molecules/cm^2) is compared to the solution spectrum with the same number of dye molecules per

unit area. The band shape and the peak position of the surface-bound RhBs did not noticeably change for the relatively small dye coverage region for up to $\sim 5 \times 10^{13}$ molecules/cm^2, so the difference in these spectral parameters from the solution spectrum can be attributed to the surface environmental effects rather than to potential dye aggregation. The more important difference between the two spectra in Figure 3 is in the overall light absorption efficiency. In more accurate terms, the frequency-integrated absorbance for the surface-bound RhB was greater by a factor of $\sim$1.5 than that for the solution spectrum. This factor (2:3 intensity ratio) strongly suggests that the surface-bound RhBs on glass are flat-on in this relatively low coverage regime with their transition moments parallel to the surface. This is reasonable considering the good planar molecular structure of RhB.

The in-plane orientations of the surface-bound RhBs on the glass surface must be still random and so would be the emission dipoles (when excited by unpolarized light at normal incidence). Then, the corresponding angular dependence of the fluorescent emission into the air half space and that into the glass medium can be calculated according to the equations given by Enderlein and co-workers.[34] The expressions suitably modified for the above condition and also to explicitly include the emission angle are given by

$$I_1(\theta) = Cn_1[\cos^2\theta(1 - R_p)^2 + (1 + R_s)^2]$$
$$0 \le \theta \le \pi/2 \quad (3)$$

$$I_2^g(\theta') = C(n_2^3/n_1^2)(\cos^2\theta'/|\cos\xi|^2)(|\cos\xi|^2|T_p|^2 + |T_s|^2)$$
$$\pi/2 \le \theta' \le \pi \quad (4)$$

Here, C is a common proportionality constant, and n_1 and n_2 represent the refractive index of air ($n_1 = 1$) and that of glass ($n_2 = 1.51$), respectively. R_p and R_s are the reflection coefficients for plane p and s waves at the air/glass interface at the angle of incidence from the air side equal to θ. The parameter ξ in eq 4 is the angle related to θ' via the following Snell's law

$$n_1 \sin\xi = n_2 \sin\theta'$$
$$\pi/2 \le \theta' \le \pi \quad (5)$$

Because $n_1 < n_2$, ξ becomes a complex angle when $\sin\theta' > n_1/n_2$. T_p and T_s in eq 4 represent the transmission coefficients (also complex numbers when $\sin\theta' > n_1/n_2$) for plane p and s waves at the angle of incidence from the air side equal to ξ. It should be noted that θ' in eq 4 is not the angle at which one detects the fluorescence signal in the backspace. The fluorescence emitted into the glass medium has to pass through the glass/air interface before being collected by the detector, thus being subjected to an additional refraction effect. The final form of the angular dependence in the backspace as corrected for this effect is obtained by substituting $I_2^g(\theta')$ for I_0 in eq 2.

$$I_2(\theta) = I_2^g(\theta')|\cos\theta|/n_2(n_2^2 - \sin^2\theta)^{1/2}$$
$$\pi/2 \le \theta \le \pi,\ n_1 \sin\theta = n_2 \sin\theta' \quad (6)$$

Figure 4 shows the comparison between the measured (point by point) fluorescent angular dependence of RhB on glass and one (solid line) that follows eqs 3 and 6. There is indeed a close agreement between them. Note that even though the additional refraction effect largely reduces the backspace fluorescence intensity (eq 6), it remains still significantly greater than that

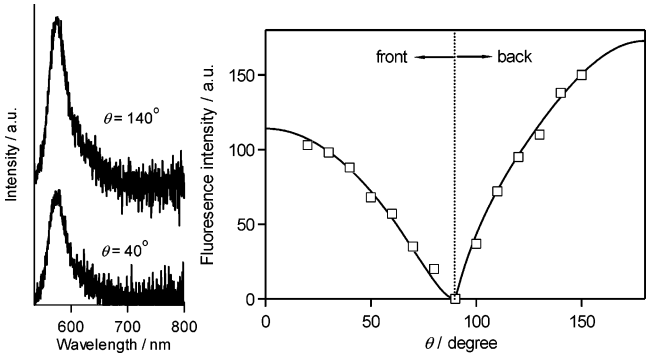

Figure 4. Fluorescence angular dependence for RhB directly coated on glass surface fitted by the theoretical one (solid line) derived according to eqs 3 and 6. Examples of fluorescence signals (excited at 532 nm) taken at two typical angles are shown on the left.

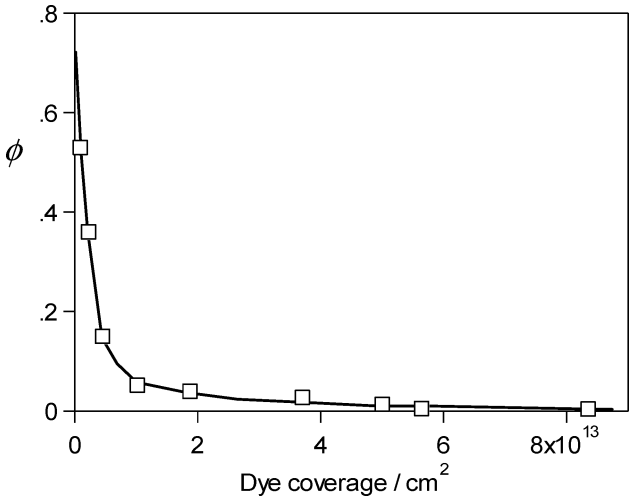

Figure 5. Absolute fluorescence quantum yield of RhB directly coated on glass surface estimated as a function of dye coverage.

in the front space. For reference, examples of the fluorescence signals used to obtain the experimental angular dependence are shown on the left of Figure 4. As compared to the solution spectra, the peak wavelength exhibited a 10-nm red shift from 568 nm but the spectral shape was approximately identical.

Together with the absorption spectra as shown in Figure 3 (which gives the net absorptance at an arbitrary excitation wavelength), the above information regarding the fluorescent angular dependence then allows us to estimate the absolute fluorescence quantum yield (ϕ) of RhB directly coated on the glass surface as a function of dye coverage. The result is as shown in Figure 5. In practice, in the limiting dye coverage region less than $\sim 5 \times 10^{12}$ molecules/cm^2, the direct measurement of the dye coverage and the corresponding dye absorptance ($<$0.005 at the peak) became increasingly more erroneous even if the fluorescence signal was still clearly observed. For the necessary data in this region, therefore, we rather relied on the good linear relationship between the dye coverage (and hence the absorptance) and the concentration of the dye solution spun on the sample surface.

In Figure 5, a strong self-quenching in the higher coverage region resulting in the low yield of the order of 0.01 or less is immediately evident. In the low coverage region below 1×10^{13} molecules/cm^2, the absolute yield then increased sharply with decreasing coverage. In this region, the average nearest neighbor distance for the surface-bound RhBs becomes greater than $\sim$30 Å, thus effectively suppressing the self-quenching due to the intermolecular energy transfer. Furthermore, Figure 5

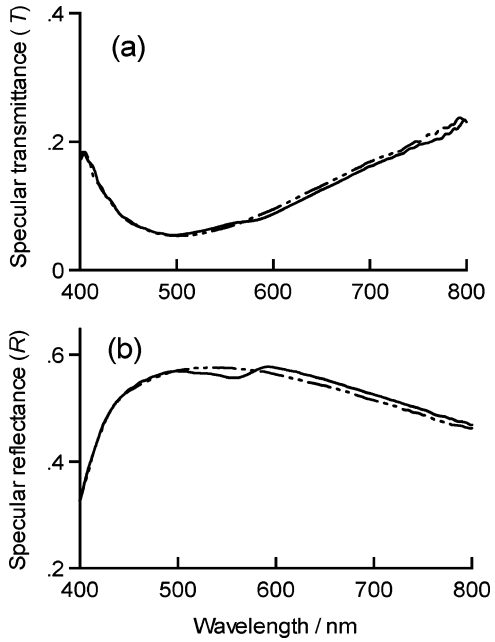

Figure 6. Typical examples of (a) specular transmittance and (b) reflectance spectra of TAIF/mica with only ~14-Å spacer (dashed curves) and those with RhB on top with the coverage of 5×10^{13} molecules/cm^2 (solid curves).

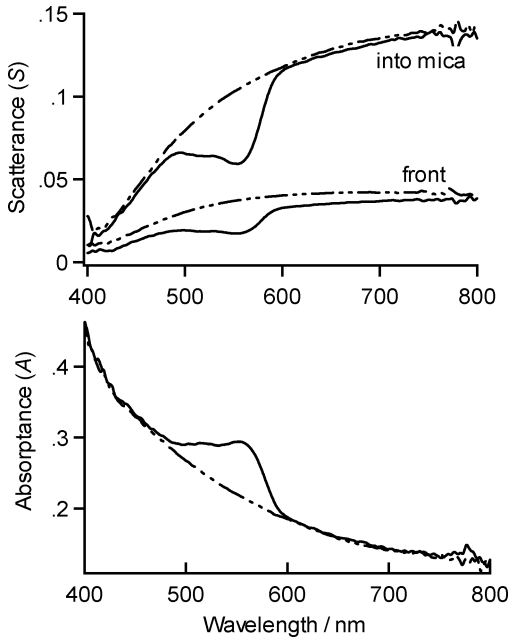

Figure 7. (a) Scattering and (b) absorptance spectra of the same samples as in Figure 6. The scattering spectra are divided into two parts scattered into the mica support and into the front half space.

suggests that the data reasonably extrapolate to a high yield somewhere above 0.6 in the low coverage limit.

Optical Properties of Dye-Coated TAIFs. The successful analysis of the fluorescence behavior of RhBs on the reference glass surface in good agreement with the available theory gives us the confidence for the quantitative examination of SEF for the RhB-coated TAIF on the same experimental grounds. Here, we first examine the optical properties of dye-coated TAIF with respect to the light absorption, reflection, and scattering for excitation at normal incidence. Figure 6 shows typical examples of the specular transmittance (T) and reflectance (R) spectra taken for TAIFs, one coated with a ~14-Å spacer only (dashed curves) and the other with also RhB at the dye coverage of 5×10^{13} molecules/cm^2 (solid curves). The spectra are not corrected for the effects of the ~0.1-mm thick mica support and thus represent the responses of dye/TAIF/mica as a whole. The corresponding spectra for the scatterance (S, a dimensionless fraction representing the absolute scattering efficiency) and the absorptance (A) are presented separately in Figure 7. In Figure 6, it can be seen that TAIF allowed minor specular transmittance, $T \sim 0.1$, in the spectral region corresponding to the RhB emission. This is attributed in large part to the high specular reflectance exceeding 0.5 characteristic of TAIF. Besides, the presence of RhB caused relatively minor changes in these spectra.

An important fact regarding the scattering spectra (Figure 7a) is that the light scattered into the backspace behind the mica substrate (across the mica/air interface) convolves the same refraction effect as does the backspace fluorescence signal. We confirmed that the angular dependence of the light scattered into the backspace (diffuse transmitted) and that into the front half space (diffuse reflected) both obeyed Lambert's cosine law. This suggests that the light initially scattered into the mica substrate also followed a simple cosine law but with the intensity greater by a factor of 2.5 (square of the refractive index of mica, 1.58) than that detected in the backspace. This relationship can be easily verified by substituting $I_0|\cos\theta'|$ (expected angular dependence of scattering into the mica substrate) for $I_2^g(\theta')$ in eq 6, which with $n_1 = 1$ leads to the following backspace angular dependence

$$I_2(\theta) = (1/n_2^2)I_0|\cos\theta| \quad (\pi/2 \le \theta \le \pi) \tag{7}$$

Figure 7a shows two separate scattering spectra, one representing the part that were scattered into the mica substrate (obtained by multiplying the backspace scatterance by a factor of 2.5 according to eq 7) and the other as measured in the front half space.

It can be seen that a much greater part of the light scattered by TAIF was distributed into the mica substrate. Furthermore, a distinct effect of RhB, largely decreasing the scatterance in the region of the dye absorption band, is now evident. This information, together with the specular transmittance and reflectance data (Figure 6), leads us to finally obtain the absorptance ($A = 1 - T - R - S$) spectra as presented in Figure 7b.

Figure 7b uncovers several unique aspects of TAIF. First, there are no distinct dipolar surface plasmon-like bands, and the absorptance shows monotonic increase with decreasing wavelength. Second, the absorptance of the dye-coated TAIF is described most likely by mere superposition of the contribution inherent to TAIF (dashed line, without RhB) and that attributed to the surface-bound RhB. This is also supported by the good agreement between the net dye absorptance spectrum derived by simple subtraction and the fluorescence excitation spectrum as shown later. The invariance of the light absorption by TAIF in the presence of the small amount of RhB (corresponding to a submonolayer coverage) is also reasonable considering the large dimensions and the overwhelming mass of the pseudotabular nanoislands as compared to the usual nanoparticles.

It should be noted, however, that this simple sum rule in the absorptance spectrum by no means suggests that the contribution of dyes is also independent of the presence of TAIF. In fact, the net dye absorptance estimated from Figure 7b was 4−5 times larger than that on the reference glass surface. Importantly, this enhanced dye absorptance is accompanied by the concomitant

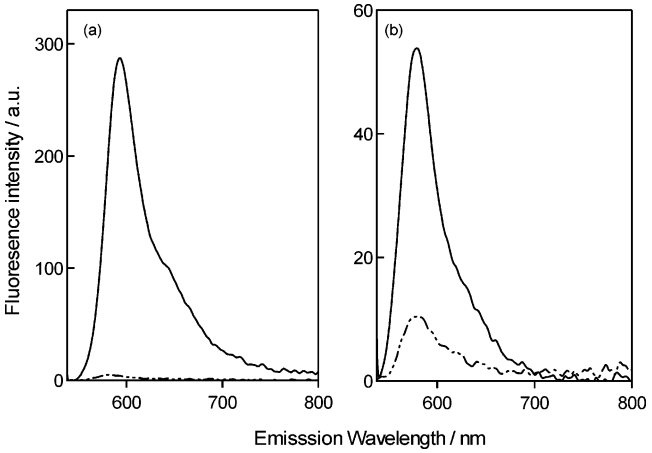

Figure 8. Comparison of fluorescence emission spectra of RhB between on reference glass surface (dashed line) and on TAIF with ~14-Å spacer, taken in the same conditions of excitation (532 nm) and detection (at $\theta = 40°$) at dye coverage of (a) 5×10^{13} molecules/cm^2 and (b) 2.5×10^{12} molecules/cm^2.

decrease of the scatterance of approximately the same magnitude (Figure 7a). This relationship suggests that the enhanced dye absorptance stemmed from the strong interactions of the dye transition dipoles with the TAIF-scattered fields. The possible orientations of the dye transition dipoles near TAIF are not necessarily clear, but we expect that RhBs are probably also flat-on around the large pseudotabular nanoislands as on the glass surface.

Analysis of SEF for RhB−Coated TAIF. Figure 8 shows typical examples of the fluorescence spectra that testify to the remarkable SEF capability of TAIF in the short range. The selected dye coverage in Figure 8a is such that the self-quenching caused a small quantum yield of ~0.01 on the glass surface, while Figure 8b corresponds to the much lower coverage where the absolute quantum yield on the glass surface increased to ~0.4 (cf. Figure 5). The spacer separating RhB from the metal surface is an only ~14-Å thick monolayer of 11-mercaptoundecanoic acid. TAIF thus caused a dramatic short-ranged enhancement by a factor of ~40 for the low quantum yield state (Figure 8a). This of course includes also the relatively minor contribution of the enhanced light absorption noted above. The apparent enhancement (by a factor of ~6) for the high quantum yield state (Figure 8b) is much smaller and may be due mostly to the enhanced excitation.

Another important aspect of this strong SEF by TAIF is with respect to its angular dependence, which was typically as shown in Figure 9. It can be seen that the fluorescence signal became considerably greater in the backspace through TAIF. If the enhanced fluorescence had originated from RhBs, then the backspace fluorescence signal should have been strongly attenuated by TAIF. The result is the opposite way around. Furthermore, the angular dependence shown in Figure 9 was very similar to that of the light scattering by TAIF not only in terms of the back/front intensity ratio but also in terms of the simple cosine law (solid lines in Figure 9) satisfied in each half space. This very intimate correlation between SEF and the light scattering by TAIF gives strong support for the view that the present SEF originated from some large induced-emission dipoles in TAIF rather than from the original dye-emission dipoles. The interesting question then is how the SEF quantum yield (ϕ_{SEF}) compares to that on the reference glass surface.

As emphasized already, the absorptance of dye-coated TAIF can be described by simple superposition of the contribution from TAIF and that from the surface-bound dye. Also, that only

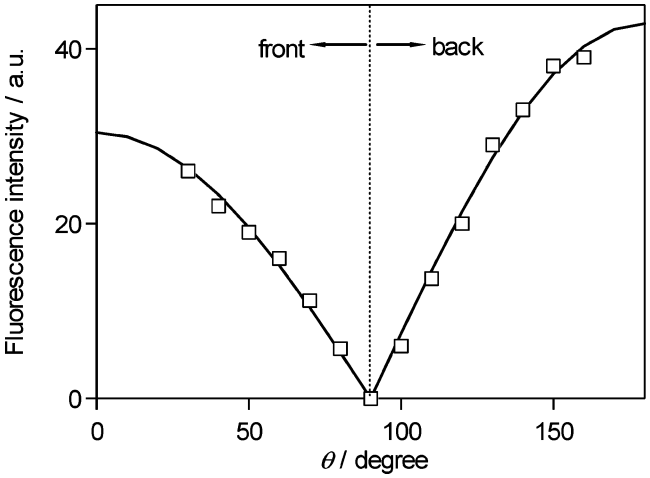

Figure 9. Typical example of angular dependence of SEF from RhB-coated TAIF. Solid lines running through the data points show angular dependences that obey a simple cosine law in each half space.

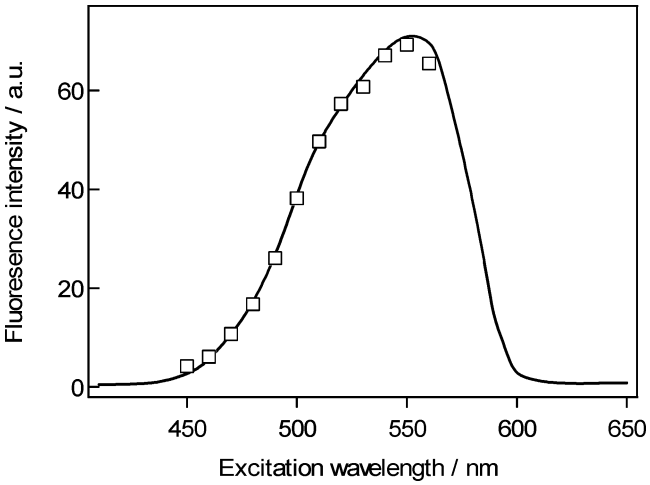

Figure 10. Example of florescence excitation spectrum measured point-by-point (squares), fitted by the net dye absorptance spectrum (solid line) for RhB-coated TAIF.

the latter part of the absorption contributed to the fluorescence excitation was confirmed by good match between the corresponding dye absorptance spectrum and the fluorescence excitation spectrum. Figure 10 shows a typical example. This lets us know the effective number of absorbed photons for the fluorescence excitation. We then have all the necessary experimental information to estimate the SEF quantum yield.

Figure 11 shows the relationship between ϕ_{SEF} and the dye coverage obtained in this way. A marked increase of the quantum yield to 0.1−0.2 (from ~0.01 or less on the glass surface) is immediately apparent in the relatively high coverage region ($2-8 \times 10^{13}$ molecules/cm^2). This relationship was apparently reversed in the lowest coverage region, but yet ϕ_{SEF} reached as high as ~0.5 in the low coverage limit. This is a markedly high yield for RhBs situated very near the metal surface. We used a spacer only ~14 Å thick to obtain the results presented so far, which is the condition where the short-ranged energy loss to the metal is normally quite strong.

The important short-ranged nature associated with the present SEF is further strengthened by the result shown in Figure 12, where we plotted also ϕ_{SEF} but as a function of spacer thickness at a relatively high dye coverage of 5×10^{13} cm^{-2}. It can be seen that even in the condition of direct contact between TAIF and RhB, there already occurred some substantial enhancement. Furthermore, it increased very steeply with increasing spacer

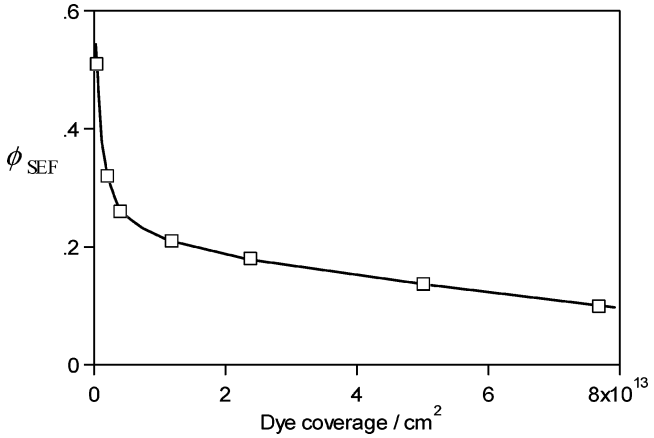

Figure 11. SEF quantum yield estimated as a function of dye coverage for RhB-coated TAIF.

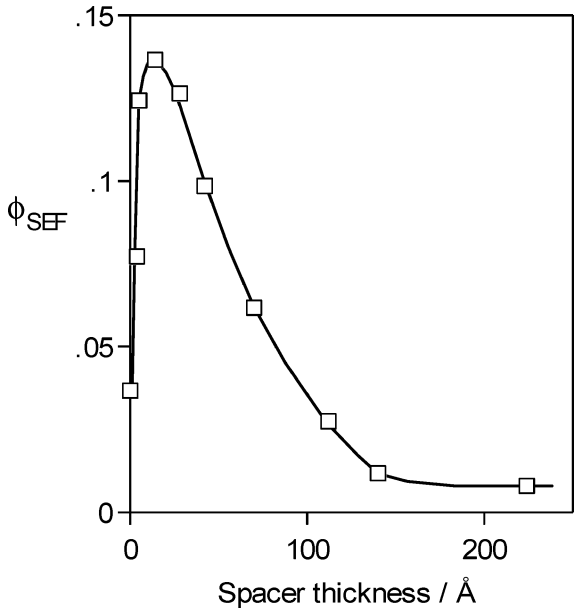

Figure 12. Estimated SEF quantum yield for RhB-coated TAIF as a function of spacer thickness. Measured at dye coverage of $\sim 5 \times 10^{13}$ molecules/cm^2.

thickness reaching the maximum at distances as short as ~10 Å. The yield then monotonically decreased with spacer thickness, and substantial enhancement in the quantum yield was observed for distances only up to ~100 Å. We interpret that the initial steep rise is probably related to the very short-ranged quenching due to the Dexter-type energy transfer to the metal involving electron tunneling. Figure 12 suggests that if this additional quenching channel had been absent, ϕ_{SEF} would have reached somewhere near 0.2 or more at the zero spacer thickness even at this comparatively high dye coverage.

Mechanism of Short-Ranged SEF by TAIF. At the short distance of ~10 Å from the metal surface, the excited dye energy must certainly be transferred very rapidly to the metal (obeying d^{-3} law) no matter what kinds of metal particles we use. The occurrence of SEF with the highest efficiency in this condition is difficult to rationalize by any other mechanism but some highly radiative decay of the energy transferred to the metal. As emphasized above, the very similar angular dependences of SEF and the light scattering by TAIF provide strong support for this mechanism. The spacer thickness of ~100 Å that mostly eliminated the present SEF also seems reasonable, if the required energy transfer coupled to the radiative mode in TAIF may not be so long ranged. This picture allows a simple kinetic description for the overall SEF quantum yield, ϕ_{SEF}, which may be expressed as

$$\phi_{SEF} = \frac{k_r}{k_r + k_{nr} + k_T} + \frac{k_T}{k_r + k_{nr} + k_T}\phi_{Ag} \qquad (8)$$

Here, ϕ_{Ag} represents the radiative yield of the induced dipole in TAIF, defined by $\Gamma_r/(\Gamma_r + \Gamma_{nr})$ with Γ_r and Γ_{nr} as the corresponding radiative and nonradiative decay rates. k_T represents the rate of dye-to-metal energy transfer relevant for producing this radiative state in TAIF. k_r is the radiative decay rate of the excited dye near TAIF, which need not be the same as that on the reference glass surface. k_{nr} is the nonradiative decay rate of the excited dye before the energy is transferred to the radiative mode of TAIF. This is due mostly to self-quenching in the case of RhB. Note, however, that near TAIF this self-quenching process can also be significantly enhanced by the metal-mediated enhanced-intermolecular energy transfer.[35] Furthermore, very near the metal surface, k_{nr} should also include the contribution of the aforementioned Dexter-type energy transfer.

At any rate, given that k_T is much larger than k_r for molecules situated sufficiently close to the metal surface, then regardless of k_{nr} the first term (representing the emission from dye) in eq 8 and k_r itself become negligible, leading to a simpler expression

$$\phi_{SEF} = \frac{k_T}{k_{nr} + k_T}\phi_{Ag} \qquad (9)$$

In the low coverage limit for RhB, the self-quenching effect can be disregarded. At the distance ~14 Å from the metal surface, the Dexter-type energy transfer would also be effectively suppressed if not completely. We then expect $k_{nr} < k_T$ in this situation, where eq 9 suggests $\phi_{SEF} \leq \phi_{Ag}$ or $\phi_{SEF} \approx \phi_{Ag}$. Thus, the SEF quantum yield in the low coverage limit, ~0.5 in Figure 11, gives a reasonable estimate of the radiative yield of the induced dipole in TAIF.

The question then is how the markedly high radiative yield, ~0.5, can be justified for TAIF. The pseudotabular Ag islands that constitute TAIF are quite large for nanoparticles, but they still may have some oscillating electromagnetic modes that can be excited by the molecular-emission dipole. The excited metal system then has a radiative decay channel due to the oscillating electric dipole moment and also a nonradiative decay channel due to the Joule heating by the oscillating electric field. In the framework of the semiclassical theory, Gersten and Nitzan pointed out the following simple inequality relationship for the corresponding decay rate,[3] which is valid for arbitrarily shaped small particles

$$\Gamma_r \leq -\frac{4\pi^2 V}{3\lambda^3}\frac{1}{Im(\epsilon - 1)^{-1}}\Gamma_{nr} \sim 600\frac{V}{\lambda^3}\Gamma_{nr} \qquad (10)$$

Here V represents the particle volume, λ the wavelength in a vacuum, and ϵ the complex dielectric constant of the particle. The approximation on the far right of eq 10 applies to Ag in the spectral region corresponding to the RhB emission. In the usual case of nanoparticles where the V/λ^3 ratio becomes extremely small (typically of the order of 10^{-5}), eq 10 forces the relationship, $\Gamma_r \ll \Gamma_{nr}$. Thus the corresponding radiative yield, $\Gamma_r/(\Gamma_r + \Gamma_{nr})$, must be very small. This means that the short-ranged coupling of molecular dipoles with the usual metal nanoparticles will invariably result in strong quenching of the fluorescence. However, eq 10 no longer imposes a severe restriction for much larger particles with the V/λ^3 ratio of the

order of 10^{-3} or higher.[3] The large pseudotabular nanoislands in TAIF indeed satisfy this condition ($V/\lambda^3 \sim 0.01$), and thus in principle eq 10 permits (never guarantees though) a high radiative yield of the induced dipole in TAIF.

Recently, Lakowicz[18] has introduced a little different terminology to account for the fact that larger Ag nanoislands can produce more enhanced fluorescence, thereby emphasizing the relationship between the absorption and scattering cross sections (related to the fluorescence quenching and enhancement, respectively) of the nanoparticles. Our present study indeed demonstrated such a close relationship between SEF and the light scattering by TAIF. Furthermore, when we more carefully compare the scattering and the absorptance spectra of TAIF (Figure 7), another interesting correlation comes up. Namely, the ratio of the scatterance to the sum of the scatterance and the absorptance, $S/(S + A)$, may serve as a simple approximate measure of the radiative yield of the induced dipoles. This ratio falls in the range of 0.4−0.6 in the region of the RhB emission wavelength (550−800 nm) according to Figure 7. This is indeed consistent with the value (∼0.5) estimated from Figure 11 on the basis of eq 9. Of course, the local electromagnetic modes as excited by the incident wave (leading to light scattering) and those by the nearby dye-emission dipoles (causing enhanced fluorescent emission) may not necessarily be identical, so the above coincidence could be yet fortuitous. It is nevertheless an interesting correlation worth investigating further, together with the possibility to gain the limiting radiative yield of $\phi_{Ag} \sim 1$. This is not very far from that already achieved by TAIF.

Summary and Conclusion

A high-temperature sputter deposition of Ag on mica produced unique TAIFs consisting of large, discrete, pseudotabular nanoislands 60−200 nm across and 30−60 nm thick. Their optical properties, particularly the remarkable short-ranged SEF capabilities for surface-bound RhBs, were addressed based on the quantitative measurements of the light absorption, reflection, scattering, and fluorescence angular distribution for excitation at normal incidence. The reliability of the angle-resolved fluorescence measurement was backed by a detailed analysis of the fluorescent behaviors of RhBs directly coated on a reference glass surface, which were fully consistent with the theory for molecular-emission dipoles situated at the interface constituting a refractive index discontinuity.

The optical properties of TAIF were characterized by a high specular reflectance in the visible region comparable to that of a continuous metal film and by no distinct dipolar surface plasmon-like band for excitation at normal incidence. As a result, the light absorption by dye-coated TAIF was a simple superposition of the contribution inherent to TAIF and that by the surface-bound dyes, though the net dye absorptance was largely increased by the interaction with the TAIF-scattered fields. The RhB-coated TAIF with a thin molecular spacer between manifested an unusually strong SEF maximized at much shorter distance from the metal surface (5−14 Å) than those hitherto known. Furthermore, considerably stronger fluorescence signals were detected in the backspace of TAIF/mica with the angular dependence very similar to that of the light scattering by TAIF.

The markedly short-ranged nature of SEF for dye-coated TAIF suggests relatively minor nonradiative energy dissipation in TAIF and that the induced emission dipole in TAIF can decay radiatively with a high yield. The estimated SEF quantum yield, ∼0.5, in the low dye coverage limit also supported this contention.

Acknowledgment. This work was supported by Kyoto Nanotechnology Cluster Project, a Grant for Regional Science and Technology Promotion from the Ministry of Education, Culture, Sports, Science and Technology, Japan

References and Notes

(1) Glass, A. M.; Liao P. F.; Bergman, J. G.; Olson, D. H. *Opt. Lett.* **1980**, *5*, 368.
(2) Ritchie, G.; Burstein, E. *Phys. Rev. B* **1981**, *24*, 4843.
(3) Gersten, J.; Nitzan, A. *J. Chem. Phys.* **1981**, *75*, 1139.
(4) Nitzan, A.; Brus, L. E. *J. Chem. Phys.* **1981**, *75*, 2205.
(5) Moskovits, M. *J. Chem. Phys.* **1982**, *77*, 4408.
(6) Weitz, D. A.; Garoff, S.; Gersten, J. I.; Nitzan, A. *J. Chem. Phys.* **1983**, *78*, 5324.
(7) Wokaun, A.; Lutz, H.-P.; King, A. P.; Wild, U. P.; Ernst, R. R. *J. Chem. Phys.* **1983**, *79*, 509.
(8) Aroca, R.; Kovacs, G. J.; Jennings, C. A.; Loutfy, R. O.; Vincett, P. S. *Langmuir* **1988**, *4*, 518.
(9) Sokolov, K.; Chumanov, G.; Cotton, T. M. *Anal. Chem.* **1998**, *70*, 3898.
(10) Tarcha, P. J.; Gonzalez, J. D.; Llorente, S. R.; Aroca, R. *Appl. Spectrosc.* **1999**, *53*, 43.
(11) Selvan, S. T.; Hayakawa, T.; Naogami, M. *J. Phys. Chem. B* **1999**, *103*, 7064.
(12) German, A. E.; Gachko, G. A. *J. Appl. Spectrosc.* **2001**, *68*, 987.
(13) Lakowicz, J. R. *Anal. Biochem.* **2001**, *298*, 1.
(14) Lakowicz, J. R.; Shen, Y.; D'Auria, S.; Malicka, J.; Fang, J.; Gryczynski, Z.; Gryczynski, I. *Anal. Biochem.* **2002**, *301*, 261.
(15) Malicka, J.; Gryczynski, I.; Gryczynski, Z.; Lakowicz, J. R. *Anal. Biochem.* **2003**, *315*, 57.
(16) Lakowicz, J. R.; Malicka, J.; D'Auria, S.; Gryczynski, I. *Anal. Biochem.* **2003**, *320*, 13.
(17) Zhang, J.; Matveeva, E.; Gryczynski, I.; Leonenko, Z.; Lakowicz, J. R. *J. Phys. Chem. B* **2005**, *109*, 7969.
(18) Lakowicz, J. R. *Anal. Biochem.* **2005**, *337*, 171.
(19) Campion, A.; Gallo, A. R.; Harris, C. B.; Robota, H. J.; Whitmore, P. M. *Chem. Phys. Lett.* **1980**, *73*, 447.
(20) Weber, W. H.; Eagen, C. F. *Opt. Lett.* **1979**, *4*, 236.
(21) Knoll, W.; Philpott, M. R.; Swalen, J. D. *J. Chem. Phys.* **1981**, *75*, 4795.
(22) Moreland, J.; Adams, A.; Hansma, P. K. *Phys. Rev. B* **1982**, *25*, 2297.
(23) Lakowicz, J. R. *Anal. Biochem.* **2004**, *324*, 153.
(24) Wedge, S.; Hooper, I. R.; Sage, I.; Barnes, W. L. *Phys. Rev. B* **2004**, *69*, 245418.
(25) Bindhu, C. V.; Harilal, S. S. *Anal. Sci.* **2001**, *17*, 141.
(26) Liang, Y.; Moy, P. F.; Poole, J. A.; Goncalves, A. M. *J. Phys. Chem.* **1984**, *88*, 2451.
(27) Kawasaki, M.; Uchiki, H. *Surf. Sci.* **1997**, *388*, L1121.
(28) Kawasaki, M. *Appl. Surf. Sci.* **1998**, *135*, 115.
(29) Evans, S. D.; Ulman, A.; Goppert-Berarducci, K. E.; Gerenser, L. J. *J. Am. Chem. Soc.* **1991**, *113*, 5866.
(30) Middleton, W. E. K.; Sanders, C. L. *J. Opt. Soc. Am.* **1951**, *41*, 419.
(31) Demas, J. N.; Crosby, G. A. *J. Phys. Chem.* **1971**, *75*, 991.
(32) Magde, D.; Wong, R.; Seybold, P. G. *Photochem. Photobiol.* **2002**, *75*, 327.
(33) Lukosz, W.; Kunz, R. E. *J. Opt. Soc. Am.* **1977**, *67*, 1607.
(34) Enderlein, J.; Ruckstuhl, T.; Seeger, S. *Appl. Opt.* **1999**, *38*, 724.
(35) Gersten, J. I.; Nitzan, A. *Chem. Phys. Lett* **1984**, *104*, 31.